Research Article

Received: 26 July 2019 Revised: 12 October 2019 Accepted article published: 21 October 2019 Published online in Wiley Online Library:

(wileyonlinelibrary.com) DOI 10.1002/pi.5936

Impact of alkyl side chain on the photostability and optoelectronic properties of indacenodithieno[3,2-*b*]thiophene-*alt*-naphtho[1,2-*c*:5,6-*c*′]bis[1,2,5]thiadiazole medium bandgap copolymers

Lili An,[a] Junfeng Tong,[b]* Chunyan Yang,[b] Xu Zhao,[c] Xunchang Wang[d] and Yangjun Xia[b]*

Abstract

Three donor-π-acceptor (D-π-A) type alternating conjugated polymers, namely PIDTT-DTNT-C16, PIDTT-DTNT-HD and PIDTT-DTNT-OD bearing the same backbone of indacenodithieno[3,2-*b*]thiophene (IDTT) as the D unit and naphtho[1,2-*c*:5,6-*c*′]bis[1,2,5]thiadiazole (NT) as the A moiety but with different flexible side chain (*n*-hexadecyl (C16), 2-hexyldecyl (HD) and 2-octyldodecyl (OD)) substituted thiophene employed as π-bridges, were synthesized and characterized. The effects of the side chain on absorption, photostability, energy levels, aggregation, backbone conformation, morphology and photovoltaic properties were systematically investigated. Because moderate D and strong A units were selected to construct the polymer backbone, a medium optical bandgap (*ca.* 1.66 eV) and low-lying highest occupied molecular orbital energy level ($E_{HOMO} \approx -5.36$ V), thus resulting in a relatively higher open-circuit voltage (V_{OC}) of 0.80–0.83 V, were achieved. It was found that the side chain gave rise to an insignificant impact on absorption, aggregation and photostability in chlorobenzene solution and energy levels but a non-negligible influence on absorption, photostability and aggregation behavior in the film state. It was found that PIDTT-DTNT-C16 with the densest and most ordered packing structure exhibited the best photostability. Inverted bulk heterojunction polymer solar cells based on PIDTT-DTNT-HD:$PC_{61}BM$ ([6,6]-phenyl-C_{61}-butyric acid methyl ester) showed at least a 1.5-fold increase in power conversion efficiency, chiefly originating from its slightly improved absorption, more balanced μ_h/μ_e ratio and favorable morphology of the active layer as a result of incorporating branched HD side chains into the IDTT-*alt*-DTNT backbone.

Supporting information may be found in the online version of this article.

Keywords: naphtho[1,2-*c*:5,6-*c*′]bis[1,2,5]thiadiazole; indacenodithieno[3,2-*b*]thiophene; alkyl side chain; aggregation; photostability

INTRODUCTION

Currently, polymer solar cells (PSCs) adopting bulk heterojunction (BHJ) architecture have attracted substantial academic and industrial enthusiasm owing to their potential advantages of low cost, light weight, flexibility in fabrication and a low temperature solution processing technique.[1–4] Such BHJ PSCs, utilizing a solution-processed active layer made up of an electron donor (D) (i.e. π-conjugated polymers) and an electron acceptor (A) (i.e. [6,6]-phenyl-C_{61}-butyric acid methyl ester ($PC_{61}BM$) or 3,9-bis(2-methylene-(3-(1,1-dicyanomethylene)indanone))-5,5,11,11-tetra(4-hexylphenyl)dithieno[2,3-*d*:2′,3′-*d*′]-s-indaceno[1,2-*b*:5,6-*b*′]dithiophene (ITIC) etc.), sandwiched between indium tin oxide (ITO) and metallic electrodes, not only can provide abundant D–A interfaces for exciton dissociation into free charges but also can form an interpenetrating network for free charge transport to the corresponding collecting electrodes.[5] Benefitting from tremendous efforts related to novel materials or new device architectures, the power conversion efficiencies (PCEs) for single junction PSCs, prepared under laboratory conditions, have already exceeded over 15%.[6,7] However, there are still challenges for PSCs

* Correspondence to: J Tong or Y Xia, School of Materials Science and Engineering, Lanzhou Jiaotong University, Lanzhou 730070, P. R. China, E-mail: tongjunfeng139@163.com (Tong); E-mail: xiayangjun2015@126.com (Xia)

a School of Chemical Engineering, Northwest Minzu University, Key Laboratory for Utility of Environment-Friendly Composite Materials and Biomass in University of Gansu Province, Lanzhou, P.R. China

b School of Materials Science and Engineering, Lanzhou Jiaotong University, Lanzhou, P. R. China

c Institute of Soil, Fertilizer and Water-saving Agriculture, Gansu Academy of Agricultural Sciences, Lanzhou, P.R. China

d CAS Key Laboratory of Bio-based Materials, Qingdao Institute of Bioenergy and Bioprocess Technology, Chinese Academy of Sciences, Qingdao, P.R. China

to meet the demand of commercialization. To further elevate the efficiency, exploring new conjugated polymers (CPs) plays a significant role. Commonly, in terms of harvesting solar energy (i.e. optical bandgaps E_g^{opt}), CP materials can be classified into three categories: low bandgap (LBG) (E_g^{opt} < 1.6 eV), medium bandgap (MBG) (E_g^{opt} 1.6 – 1.8 eV) and wide bandgap (WBG) (E_g^{opt} > 1.8 eV).[5,8] Recently, most successful donor CPs for solar cell application have been designed to be LBG materials because, the lower the bandgap, the more sunlight can be absorbed, which can broaden the absorption to extend to the near-infrared region and acquire higher short-circuit current density (J_{SC}). However, it was unreasonable to over-approach the highest occupied molecular orbital (HOMO) energy level (E_{HOMO}) and the lowest unoccupied molecular orbital (LUMO) energy level (E_{LUMO}). Elevating the HOMO level may reduce the open-circuit voltage (V_{OC}); meanwhile the E_{LUMO} level was higher (usually larger than about 0.3 eV) than the electron acceptor so as to supply enough driving force for charge separation.[2] Additionally, the intrinsic narrow absorption bands for LBG CPs would limit broad photon harvesting and prevent making full use of the entire solar spectrum.[3] Compared to the well-developed LBG counterparts, the development of MBG and WBG copolymers are less important. Nevertheless, they are still of importance for PSCs because the MBG and WBG copolymers can match with the non-fullerene electron acceptors so as to simultaneously obtain complementary absorption and a deeper E_{HOMO}, and thus obtain both enhanced J_{SC} and V_{OC} of PSCs.[9] Meanwhile, they are also used as vital components in tandem devices and can facilitate tandem cells to harvest more solar light.[10] Therefore, it is highly desirable to design WBG and MBG CPs and further understand the structure–property relationships governing the material performance.

Solution-processed CPs mainly contain π-conjugated backbones and flexible solubilizing side chains hung perpendicularly.[11–14] The most successful strategy to construct the π-conjugated backbones of CPs is by incorporating an electron-rich (D) moiety and an electron-deficient (A) unit and alternating them in their repeating units via molecular orbital hybridization, which can take advantage of photo-induced intramolecular charge transfer (ICT) from D to A, and the bandgap, hole mobility and electron energy levels can be easily tuned by finely selecting the D and A units.[15–28] Beyond tuning the conjugated backbones of CPs, selecting suitable side chains is also a viable and effective method for elevating the efficiency. The roles of the side chains are not confined to molecular weight, solubility and solution-processed properties. In fact, the number, branch, length and rigidity of the side chains as well as the position of the CP frameworks have an increasing impact in regulating the optical absorption, thermal stability, photostability, crystallinity, molecular orientation and morphology in the active layers.[12,14,29–37] Recently, many efforts have been devoted to comprehending the effect of the side chain on the functional and optoelectronic properties of CPs. Studies of well-known poly(3-alkylthiophene)s have shown that not only the length of the alkyl side chain affects the solubility but also a longer one decreases the absorbance, stacking and hole mobility.[31] Wang *et al.* prepared three CPs bearing a carbazole-thiophene-quinoxaline-thiophene backbone and tuned the shape and length of the side chain; they found that poly{9-octylcarbazole-2,7-diyl-*alt*-5,8-bis(thien-2-yl)-2,3-bis(3-(octyloxy)phenyl)quinoxaline-5,5′-diyl} (EWC3) bearing the largest side chain yielded the highest PCE and V_{OC}.[32] Beaujuge and colleagues changed the size and branching position of the side chains in the poly{benzo[1,2-*b*:4,5-*b*′]dithiophene-*alt*-thieno[3,4-*c*]pyrrole-4,6-dione} (PBDT-TPD) family and found that the polymer backbone orientation exhibited a critical change, i.e. the preferential 'face-on' disappeared and thus the PCE was lowered when the branched chain was replaced by a linear one.[33] Li *et al.* found that the width of the fibrillar microstructure of blend films was decreased which could facilitate exciton dissociation, and thus the shortest-chain-containing poly{*N*,*N*-di(2-hexyldecyl)diketopyrrolopyrrole-*alt*-thiophene-phenylene-thiophene} (HD-PDPPTPT) yielded the best PCE of 7.4%, with decrease of the side chain length in the crystalline poly{diketopyrrolopyrrole-*alt*-thiophene-phenylene-thiophene} (PDPP-TBT) family CPs.[34] Huang and colleagues studied two naphtho[1,2-*c*:5,6-*c*′]bis[1,2,5]thiadiazole-based CPs and shortened the spacer's side chain from 2-decyltetradecyl (DT) (NT1014) to 2-octyldodecyl (OD) (NT812), which induced the formation of the favorable 'face-on' orientation, and thus the PCE was remarkably enhanced from 3.03% to 10.33%.[35] Recently, our group found that a tiny change of alkyl side chain (from 2-hexyldecyl (HD) to OD) in the poly[4,8-bis[5-(2-butyloctyl)thieno[3,2-*b*]thien-2-yl]benzo[1,2-*b*:4,5-*b*′]dithiophene-2,6-diyl-*alt*-4,9-bis(thien-2-yl)naphtho[1,2-*c*:5,6-*c*′]bis[1,2,5]thiadiazole-5, 5′-diyl] (PBDT-TT-DTNT) family enhanced the PCE, owing to 2-fold higher mobility, favorable phase separation and enhanced exciton dissociation.[14] It was not difficult to see that the correlation between side chain structure and photovoltaic (PV) properties was complicated and it was premature to draw effect laws; therefore it was of crucial importance to precisely make a balance between the side chain of CPs, solution processability, backbone, stacking, charge transport, morphology and PV performance.

Recently, highly fused electron arenes have been widely focused on and exhibited appealing optoelectronic applications.[38–41] By fastening or fusing adjacent rings, the rigid backbones can be extended horizontally or vertically. It has been demonstrated that highly fused aromatic/heteroaromatic units not only can enhance the effective conjugation and overlap of π-orbitals along the polymer backbone to facilitate electron delocalization, which is propitious for acquiring a red-shifted absorption spectrum, but can also be conducive to intermolecular charge carrier hopping and restraining the interannular rotation in order to reduce the Marcus reorganization energy, resulting in an improved intrinsic charge mobility.[42–49] Among the numerous D units, one appealing D moiety is a penta-ring indacenodithiophene (IDT) and plenty of IDT-based CPs with excellent PV performance have been reported.[42,43,50,51] Xu *et al.* found that the PCE was increased from 5.97% to 7.03% as a result of an improved mobility of the longer effective conjugation and better planarity evoked by a hepta-ring indacenodithieno[3,2-*b*]thiophene (IDTT) unit by extending π-conjugation along the IDT linear backbone.[43] Cai *et al.* also demonstrated that a 1,3-bis(thien-2-yl)-5,7-bis(2-ethylhexyl)benzo[1,2-*c*:4,5-*c*′]dithiophene-4, 8-dione (T1)-based CP IDTT-T1 exhibited 5.5-fold higher field-effect transistor mobility than that of IDT-T1 and thus the PCE was raised from 6.26% to 6.58%.[44] Furthermore, the hepta-ring of IDTT was expanded to an undeca-ring IDT-biscyclo-pentadithiophene (IDTCPDT) by Li *et al.* and it was found that fully rigidified difluorobenzothiadiazole (DFBT)-based CP PIDTCPDT-DFBT exhibited a wider and stronger absorption band, a reduced reorganizational energy from 4.1 to 3.2 kcal mol^{-1} and a 1-order-elevated hole mobility; thus the J_{SC} was increased from 10.40 to 14.59 mA cm^{-2},[49] which made these IDTT-based CPs gain particular interest.[43–49,52–56] Among the many electron acceptor units, a tetracyclic heteroaromatic ring

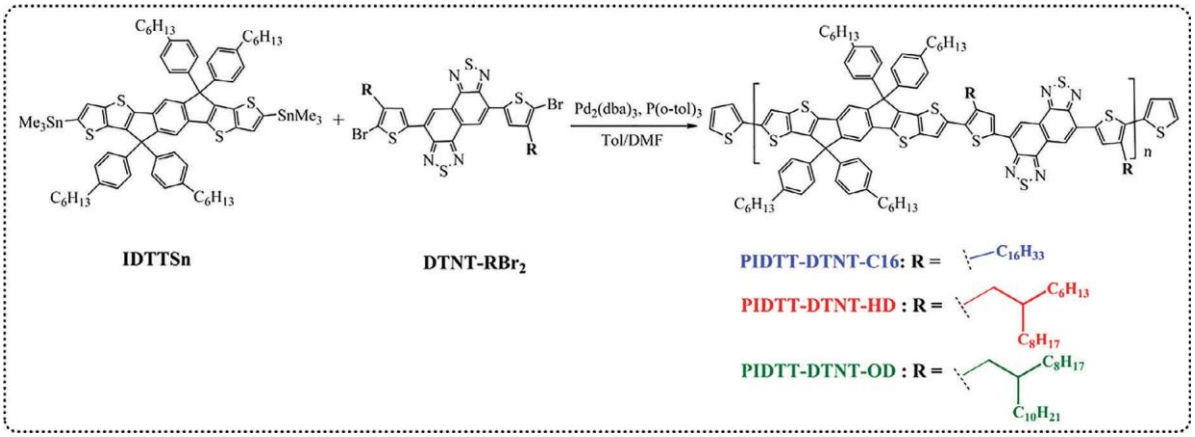

Scheme 1. Syntheses of copolymers PIDTT-DTNT-C16, PIDTT-DTNT-HD and PIDTT-DTNT-OD.

naphtho[1,2-*c*:5,6-*c*′]bis[1,2,5]thiadiazole (NT) fused by double benzothiadiazole (BT) rings, exhibiting an enlarged planarity and stronger electron-accepting ability has been widely applied in the PV field.[24,35,57–64] For example, excellent NT was first introduced into the polymer backbone instead of BT by Huang's group; it was found that PBDT-DTNT exhibited a remarkably extended absorption profile, decuple higher charge mobility and therefore 2.84 times higher PCE than its counterpart PBDT-DTBT even though a decreased V_{OC} resulted from an elevated E_{HOMO}.[58] Furthermore, another NT-based star material was composed of DTNT and 2,2'-bithiophene moieties, or composed of NT and tetrathiophene (PNTz4T) combining NT with the electron-richer oligothiophene tetrathiophene was developed by Osaka's group and showed a narrower bandgap, a lower-lying E_{HOMO}, a more highly ordered structure and thus a 2.48 times enhanced PCE compared to PBTz4T.[59] Recently, we utilized NT to replace BT in triisopropylsilylethynyl substituted dithienobenzodithiophene-based CPs, and the PCE was enhanced by 1.29 times originating from greatly widened absorption, deepened E_{HOMO}, better coplanarity and elevated mobility, as well as the favorable morphology in the active layer.[64] Based on the above facts, it is of importance to synthesize CPs containing the hepta-ring fused IDTT moiety and an NT unit bearing a highly □-extended structure and stronger electron affinity and to further attempt to make a thorough inquiry into the structure– property correlation.

In consideration of the desirable properties of IDTT and NT moieties, herein, a family of D-□-A type MBG CPs containing different flexible side chains *n*-hexadecyl (C16), HD and OD of □-bridge thiophene, namely PIDTT-DTNT-C16, PIDTT-DTNT-HD and PIDTT-DTNT-OD, respectively, in which fused hepta-ring IDTT and centrosymmetric NT moieties are used as D and A units (Scheme 1), were synthesized to systematically investigate the impact of the side chain on the photophysical properties, photostability, electrochemical properties, backbone conformation and PV properties. A medium ICT interaction was formed, leading to an MBG of approximately 1.66 eV which is close to that of PIDT-DTNT (1.65 eV)[50] but smaller than that of PIDTT-DTFBT-T,[56] owing to the combination of the strong A unit of NT with the medium D of IDTT. It was found that the side chain gave rise to an insignificant impact on absorption and photostability in chlorobenzene (CB) solution and energy levels but a non-negligible influence on absorption, photostability and aggregation in the film state. It was found the PIDTT-DTNT-C16 with linear side chain exhibited the best photostability, while the PIDTT-DTNT-HD:$PC_{61}BM$ based device showed the best PCE, which was obviously higher than those containing the other two side chains (C16 and OD).

EXPERIMENTAL

Measurement and characterization

^{1}H NMR spectra, melting point tests, C, H and N elemental analyses, TGA analyses, molecular weight of the polymers, UV – visible absorption, electrochemical properties, and AFM and TEM images were obtained according to our reported methods.[24] The photostability of the polymers and XRD were measured according to our reported methods.[25]

Materials

All utilized chemical reagents were reagent grade and were purchased from J&K Scientific, TCI Chemical Co. and Sigma-Aldrich Co. and were used without further purification. Solvents such as tetrahydrofuran, *n*-hexane and diethyl ether (Et_2O) were dried over sodium/benzophenone and freshly distilled prior to use. 4,9-Bis(5-bromo-4-(2-hexyldecyl)thien-2-yl)naphtho[1,2-*c*:5,6-*c*′]bis[1,2,5]thiadiazole (DTNT-$HDBr_2$), 4,9-bis(5-bromo-4-(2-octyldodecyl)thien-2-yl)naphtho[1,2-*c*:5,6-*c*′]bis[1,2,5]thiadiazole (DTNT-$ODBr_2$)[14,24] and polyelectrolyte poly[(9,9-bis-(3′-(*N*,*N*-dimethylamino)propyl)- 2,7-fluorene)-*alt*-2,7-(9,9-dioctylfluorene)] (PFN)[65] were synthesized according to the corresponding references. 2,8-Bis(trimethyltin)-6,6,12,12-tetra(4-hexylphenyl)indacenodithieno[3,2-*b*]thiophene (IDTTSn)[43,66] and 4,9-bis(5-bromo-4-(*n*-hexadecyl)thien-2-yl)naphtho[1,2-*c*:5,6-*c*′]bis[1,2,5]thiadiazole (DTNT-$C16Br_2$) were synthesized as described in Appendix S1.

Synthesis procedures

The general procedure adopted for polymer synthesis was as follows. Carefully purified bistin monomer IDTTSn and dibromo-monomer (DTNT-$C16Br_2$, DTNT-$HDBr_2$ and DTNT-$ODBr_2$) were dissolved into 6 mL degassed dry toluene and 0.8 mL *N*,*N*-dimethylformamide (DMF) in a 25 mL two-neck round-bottom flask under Ar. The mixture was bubbled with Ar for an additional 20 min to remove O_2. Thereafter, $Pd_2(dba)_3$ (1.4 mg) and P(*o*-tolyl)$_3$ (2.3 mg) were quickly added to the mixture in one portion and the solution was bubbled with Ar for another 20 min. The mixture was then vigorously refluxed for 48 h under Ar, followed by the subsequent addition of 2-tri(butylstannyl)thiophene and 2-bromothiophene at an interval of 8 h for end-capping. After

refluxing for an additional 8 h, the mixture was poured into 300 mL methanol. The precipitate was collected by filtration and the crude polymer was subjected to Soxhlet extraction successively with ethanol, acetone, hexane and toluene. The toluene fraction was condensed to about 6 mL and precipitated into methanol. The black solid was collected and completely dried under vacuum overnight to obtain the target material with yields of 83.3%–92.3%.

*Synthesis of poly[6,6,12,12-tetra(4-hexylphenyl)indacenodithieno [3,2-b]thiophene-2,8-diyl- alt-4,9-bis(4-(*n*-hexadecyl)thien-2-yl) naphtho[1,2-c:5,6-c′]bis[1,2,5]thiadiazole-5,5′-diyl]*
(***PIDTT-DTNT-C16***)

IDTTSn (134.5 mg, 0.10 mmol) and DTNT-C16Br$_2$ (101.5 mg, 0.10 mmol) were used to prepare PIDTT-DTNT-C16 according to the general procedure illustrated above. A black solid with metallic luster of about 172.8 mg (PIDTT-DTNT-C16) was obtained with a yield of 92.3%.

Number-average molecular weight (M_n) = 29.4 kDa, polydispersity index (PDI) 2.5. ^{1}H NMR (400 MHz, $CDCl_3$), □ (ppm): 9.08 (br, ArH), 8.17 (br, ArH), 7.55 (br, ArH), 7.47 (m, ArH), 7.24 (m, ArH), 7.15 (br, ArH), 7.13 (br, ArH), 2.84 (br, CH_2), 2.59 (m, CH_2), 1.85 (br, CH_2), 1.61 (br, CH_2), 1.35–1.20 (m, CH_2), 0.85–0.82 (m, CH_3). Analysis calculated for $C_{118}H_{142}N_4S_8$: C, 75.67%; H, 7.64%; N, 2.99%. Found: C, 75.51%; H, 7.50%; N, 3.10%.

Synthesis of poly[6,6,12,12-tetra(4-hexylphenyl)indacenodithieno [3,2-b]thiophene-2,8-diyl- alt-4,9-bis(4-(2-hexyldecyl)thien-2-yl) naphtho[1,2-c:5,6-c′]bis[1,2,5]thiadiazole-5,5′-diyl]
(***PIDTT-DTNT-HD***)

IDTTSn (172.8 mg, 0.128 mmol) and DTNT-HDBr$_2$ (130.4 mg, 0.128 mmol) were used and the polymer PIDTT-DTNT-HD was collected as a black solid with metallic luster (209.7 mg). Yield 87.2%. M_n = 32.4 kDa, PDI = 2.2.

^{1}H NMR (400 MHz, $CDCl_3$), □ (ppm): 9.07 (br, ArH), 8.17 (br, ArH), 7.55 (br, ArH), 7.48 (m, ArH), 7.24 (m, ArH), 7.15 (br, ArH), 7.13 (br, ArH), 2.85 (br, CH_2), 2.59 (m, CH_2), 1.85 (br, CH), 1.61 (br, CH_2), 1.35–1.20 (m, CH_2), 0.87–0.80 (m, CH_3). Analysis calculated for $C_{118}H_{142}N_4S_8$: C, 75.67%; H, 7.64%; N, 2.99%. Found: C, 75.61%; H, 7.42%; N, 3.05%.

Synthesis of poly[6,6,12,12-tetra(4-hexylphenyl)indacenodithieno [3,2-b]thiophene-2,8-diyl- alt-4,9-bis(4-(2-octyldodecyl)thien-2-yl) naphtho[1,2-c:5,6-c′]bis[1,2,5]thiadiazole-5,5′-diyl]
(***PIDTT-DTNT-OD***)

IDTTSn (144.5 mg, 0.107 mmol) and DTNT-ODBr$_2$ (121.4 mg, 0.107 mmol) were used. The polymer PIDTT-DTNT-OD was collected as a black solid with metallic luster (177.0 mg, yield 83.3%). M_n = 34.3 kDa, PDI = 2.1.

^{1}H NMR (400 MHz, $CDCl_3$), □ (ppm): 9.03 (br, ArH), 8.17 (br, ArH), 7.56 (br, ArH), 7.47 (m, ArH), 7.25 (m, ArH), 7.16 (br, ArH), 7.14 (br, ArH), 2.88 (br, CH_2), 2.60 (m, CH_2), 1.79 (br, CH), 1.61 (br, CH_2), 1.35–1.20 (m, CH_2), 0.87 (br, CH_3). Analysis calculated for $C_{126}H_{158}N_4S_8$: C, 76.23%; H, 8.02%; N, 2.82%. Found: C, 76.01%; H, 7.81%; N, 2.70%.

Fabrication and characterization of the photovoltaic cells

The detailed procedure for fabrication and characterization of the PSCs is given in Appendix S1.

Hole-only and electron-only device fabrication and measurement

The detailed procedure for hole-only and electron-only devices[64,67] is also given in Appendix S1.

RESULTS AND DISCUSSION

Synthesis and characterization

The general synthetic route for bistin comonomer IDTTSn, including the three steps Negishi coupling, double nucleophilic addition-intramolecular Friedel–Crafts annulation, and distannylation, is depicted in Appendix S1, Scheme S1, according to references[43,66]. The yields of these synthetic procedures were 80%, 65% and 80%, respectively. Furthermore, dibromide DTNT-C16Br$_2$ was synthesized according to our reported method.[14,24] These key intermediates and comonomers have been characterized and identified by NMR (Appendix S1, Figs S1–S5) and elemental analyses. Note that an increase of 20 °C in the melting point for DTNT-C16 after dibromination was found; more importantly, ^{1}H NMR of DTND-C16Br$_2$ was detected in *o*-dichlorobenzene-d4 (*o*-DCB-d4) because of poor solubility at elevated temperature (Appendix S1, Fig. S5), demonstrating that DTNT-C16Br$_2$ had been successfully brominated. As elucidated in Scheme 1, the resultant copolymers PIDTT-DTNT-C16, PIDTT-DTNT-HD and PIDTT-DTNT-OD were prepared by means of typical Stille polymerization utilizing $Pd_2(dba)_3$ and tri(*o*-tolyl)phosphine as the catalyst system in toluene/DMF solution.[68] At the end of polymerization, end-capping was performed with 2-tri(butylstannyl)thiophene and 2-bromothiophene for enhancing the copolymer stability.[69] Purification of the resulting copolymers was carried out by our reported method.[24] Finally, the toluene-soluble fraction was recovered by re-precipitation in MeOH and then dried under vacuum overnight to remove the residual solvents. All polymers were obtained as black metallic luster solids with higher yields of 83.3%–92.3%. Furthermore, these resultant copolymers had good solubility in chlorinated solvents such as chloroform, CB and *o*-dichlorobenzene, which satisfied the requirements for solution-processed fabrication for PSCs.

The structures of the obtained copolymers were identified by ^{1}H NMR spectra, as shown in Appendix S1, Figs S6–S8. Three copolymers showed the distinct ^{1}H NMR signal in the aromatic regions. The peaks in the range of 9.08–9.02 ppm can be attributed to aromatic hydrogen of the NT core and those at 8.16–8.17 ppm can be ascribed to aromatic hydrogen of different flexible side chain substituted thiophene spacers. Meanwhile, peaks situated at 7.56–7.46 ppm can be assigned to aromatic hydrogen of the IDTT core and those at 7.24–7.12 ppm were assigned to aromatic hydrogen of hexylphenyl attached to IDTT. The peaks located at 2.84–2.88 ppm belonged to the signal of CH_2 directly linked to the thiophene spacer and those at 2.60–2.57 ppm originated from the signal of CH_2 directly linked to the hexylphenyl group. The peaks at 1.61–0.80 ppm were ascribed to the signals of remaining CH_2 and CH_3 of the flexible side chains. Moreover, the results of elemental analysis were also in accordance with the theoretical values. M_n values of the resultant PIDTT-DTNT-based copolymers were tested by gel permeation chromatography (Table S1 in Appendix S1). The values of M_n and the PDIs were found to be approximately 32.4 kDa and 1.8 for PIDTT-DTNT-C16, 31.2 kDa and 1.9 for PIDTT-DTNT-HD, and 34.4 kDa and 2.1 for PIDTT-DTNT-OD, respectively. These copolymers had similar molecular weights, so the particular effect of molecular weight on property could be overlooked. We measured the thermal properties of these copolymers through TGA. From Fig. S9 and Table S1 in Appendix S1, three copolymers exhibited a decomposition temperature (T_d, 5% weight-loss temperature) over 340 °C, which can guarantee the fabrication of devices in PSCs.

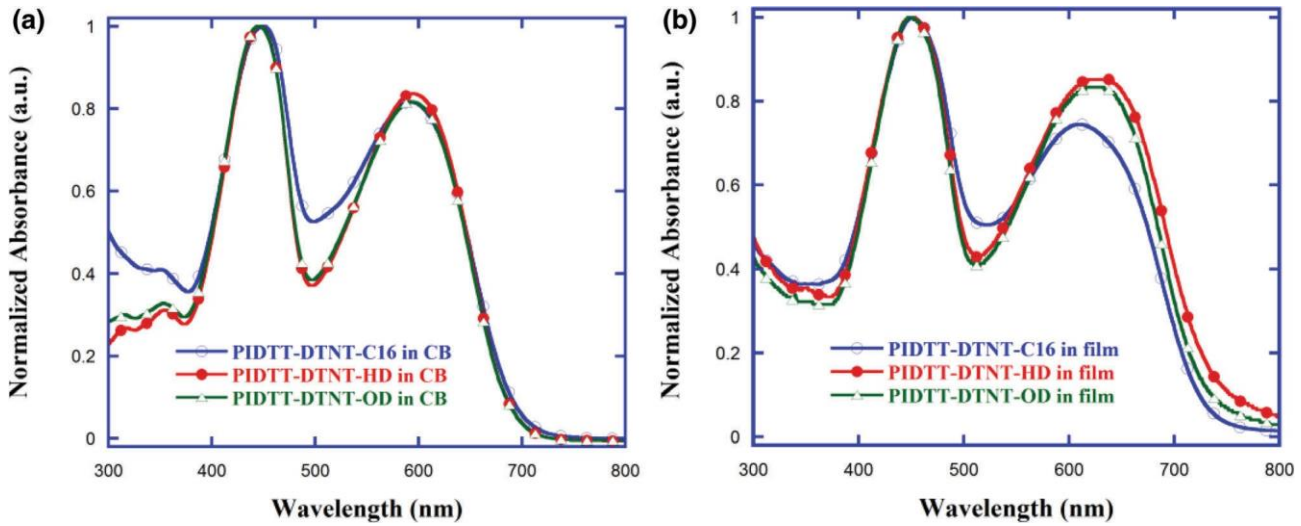

Figure 1. Normalized UV–visible absorption spectra of copolymers PIDTT-DTNT-C16, PIDTT-DTNT-HD and PIDTT-DTNT-OD in dilute CB solution (a) and as a thin film spin-cast from CB (b).

Table 1. Optical and electrochemical data of the studied copolymers PIDTT-DTNT-C16, PIDTT-DTNT-HD and PIDTT-DTNT-OD

	Solution	Film					
Polymer	λ_{max} (nm)	λ_{max} (nm)	λ_{onset} (nm)	$E_g^{opt a}$ (eV)	E_{ox}^{onset} (V)	E_{HOMO} [b] (eV)	E_{LUMO} [c] (eV)
PIDTT-DTNT-C16	448, 593	454, 610	742	1.67	0.68	−5.36	−3.69
PIDTT-DTNT-HD	446, 595	450, 628	750	1.65	0.68	−5.36	−3.71
PIDTT-DTNT-OD	446, 595	450, 625	746	1.66	0.70	−5.38	−3.72

[a] Optical bandgap calculated from the onset of the film in absorption ($E_g^{opt} = 1240/\lambda_{onset}^{film}$).
[b] E_{HOMO} calculated from the oxidation potential for the copolymer ($E_{HOMO} = -e(E_{ox}^{onset} + 4.68)$ (eV)).
[c] E_{LUMO} calculated from E_g^{opt} and E_{HOMO} for the copolymers: $E_{LUMO} = E_{HOMO} + E_g^{opt}$ (eV).

Optical properties

In order to determine the effects of the side chains on the optoelectronic properties of the synthesized IDTT-*alt*-DTNT-based copolymers, the normalized UV– visible absorption spectra of each copolymer in a CB solution and as thin films are shown in Fig. 1; the summarized data are also listed in Table 1. It was observed that there were two obvious absorption bands for the three studied copolymers both in CB solution and as solid films. These short-wavelength absorbance bands ranging from 380 to 500 nm could be ascribed to a delocalized π–π* transition of the polymer backbone, while relatively weaker bands ranging from 500 nm to 750 nm in the long-wavelength region could be attributed to the ICT from electron-rich IDTT units to electron-deficient NT moieties.[50,52] In the CB solution, three CPs exhibited similar absorption profiles with maximum absorption peak at 446–448 nm and a secondary peak at *ca* 593 nm. Ongoing from solution to film, a red-shifted tendency for both π–π* and ICT transition peaks of the resultant CPs were observed. Interestingly, a pronounced red-shift by 35 nm from 593 to 628 nm for PIDTT-DTNT-HD, a medium red-shift by 30 nm from 595 to 625 nm for PIDTT-DTNT-OD and the weakest red-shift by 17 nm from 593 nm to 610 nm for PIDTT-DTNT-C16 were observed, indicating that PIDTT-DTNT-C16 exhibited the strongest solid aggregation trend, which was identical with the later XRD and density functional theory (DFT) calculation. Furthermore, the optical bandgaps (E_g^{opt}) for PIDTT-DTNT-C16, PIDTT-DTNT-HD and PIDTT-DTNT-OD were calculated to be 1.67, 1.65 and 1.66 eV, respectively, using the equation $E_g^{opt} = 1240/\lambda_{onset}^{film}$. It should be noted that the bandgap was close to the IDT-based CP PIDT-DTNT[50] but obviously smaller than the BT-based PIDTT-DFBT-T of 1.75 eV,[56] suggesting that an electron-withdrawing unit (DTFBT *versus* DTNT) has more impact on the absorption property than an electron-rich unit (IDT *versus* IDTT) in this copolymer family. In addition to the absorption profile, the absorption coefficient was another important factor used for judging the ability of harvesting solar light energy for the CPs.[14,24,64] Therefore, the molar absorption coefficients (ε_{soln} and ε_{film}) of these studied CPs both in CB solution and as solid film were measured, as shown in Figs S10 and S11 in Appendix S1. It was shown that when the side chain was changed from C16 to HD to OD, the absorption coefficient in CB solution exhibited a decreased trend (from 83 731 to 81 183 to 71 387 L mol^{-1} cm^{-1}), while the absorption coefficient in the film state was first slightly enhanced and then decreased (from 16 323 to 16 611 to 14 721 cm^{-1}), implying that the type and length of the flexible side chain had little impact on the absorption profile and coefficient. The relatively larger decrease of ε_{film} in the PIDTT-DTNT-OD film may be affected by its relatively weak molecular aggregation obtained from the XRD analysis (later). Overall, PIDTT-DTNT-HD exhibited a slightly wider absorption and enhanced absorption compared with the other two polymers in the solid film state.

It has been proved that the molecule motions of CPs are bound to be accelerated with an elevating temperature, which leads

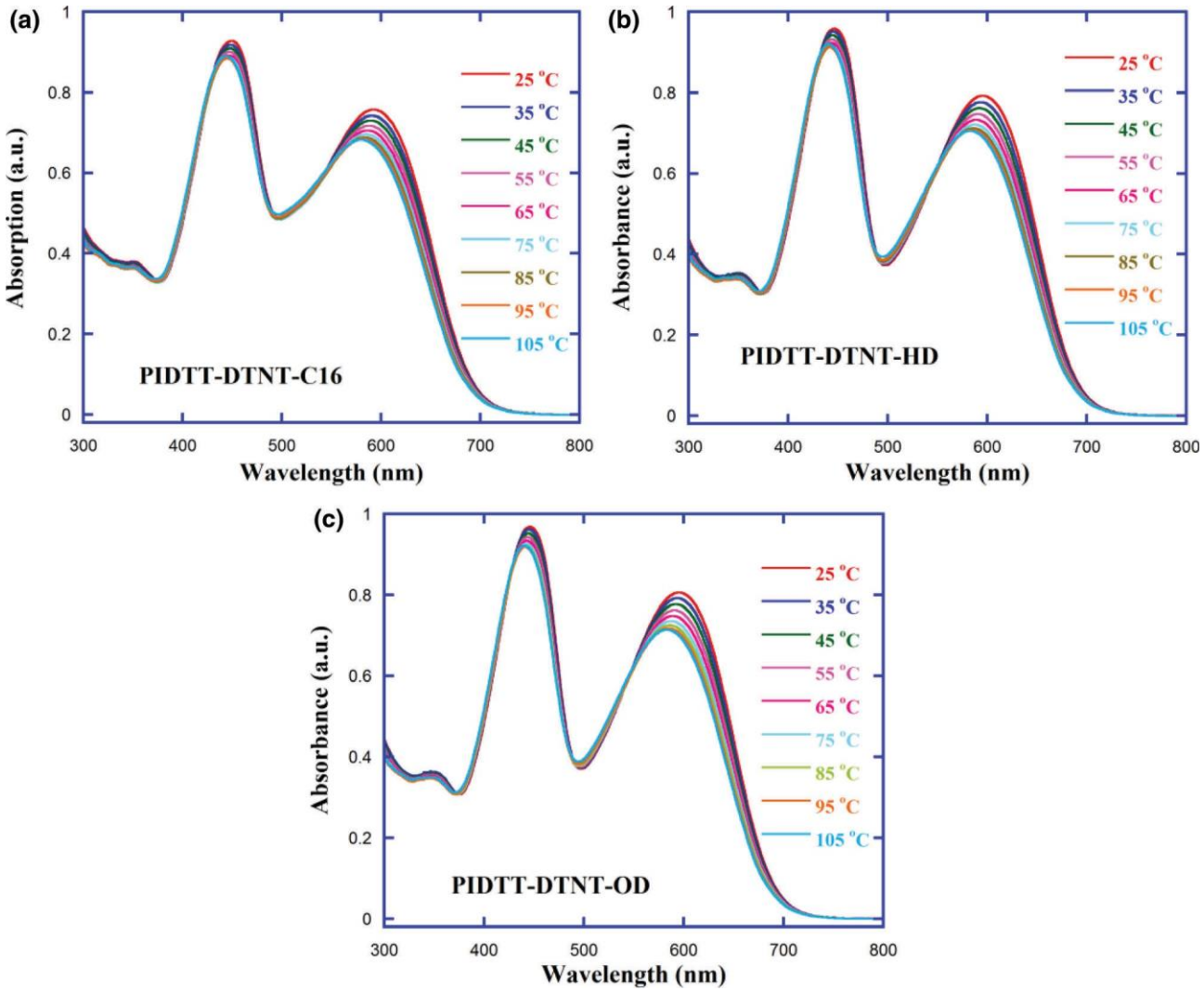

Figure 2. Temperature-dependent absorption spectra for the resultant copolymers PIDTT-DTNT-C16, PIDTT-DTNT-HD and PIDTT-DTNT-OD in CB with a concentration of about 10^{-5} mol L^{-1}.

to a reduction of the absorption shoulder peaks connected to the aggregation caused by the intermolecular □–□* transition. That is, the distortion of the conjugated backbone is intensified at an elevated temperature, resulting in a reduction of the effective conjugation length for the polymer backbone, and thus the absorption peaks produced by the delocalized □–□* transitions and those emerging by ICT transitions are both blue-shifted.[14,24,64] To gain insight into the aggregation variations of different side chains, temperature-dependent absorption spectra of the synthesized copolymers PIDTT-DTNT-C16, PIDTT-DTNT-HD and PIDTT-DTNT-OD in CB solution were measured from 25 to 115 °C with a 10 °C interval, as depicted in Fig. 2. It was shown that, when the temperature was elevated, the three copolymers showed a similar trend, i.e. the ICT and □–□* absorption peaks were both blue-shifted and both the absorption intensities decreased. In detail, the blue-shifted value and the decreased absorption intensity were 12.5 nm (from 592.5 to 580.0 nm) and 9.9% for PIDTT-DTNT-C16, 13.0 nm (from 595.5 to 582.5 nm) and 10.8% for PIDTT-DTNT-HD and 12 nm (from 595.5 to 583.5 nm) and 11.1% for PIDTT-DTNT-OD. It was concluded that the side chains had a tiny impact on the aggregation ability in CB solution.

Photostability

Apart from the ability to harvest sunlight for semiconducting copolymers, photostability is also an important issue because it is the basic requirement for commercialization of PSCs.[25,70–73] Thus, in order to inspect the effect of the side chains on the photostability, we examined the absorption changes of the studied copolymers by exposing the diluted CB solution and polymer films with thickness approximately 90 nm under AM 1.5 sunlight irradiation in air at ambient temperature. All films were prepared by spin-coating CB solution containing each polymer (*ca* 12 mg mL^{-1}) onto pre-cleaned ITO/glass substrates. As shown in Fig. S12 in Appendix S1, the three copolymers exhibited a similar variation, i.e. the ICT absorption peak decreased and blue-shifted, and the □ – □* peak only decreased with an increase of the exposure time in CB solution. As seen from Fig. S12(d), after photo-degradation for 4 h, PIDTT-DTNT-C16, PIDTT-DTNT-HD and PIDTT-DTNT-OD maintained 79.6%, 79.6% and 81.1% respectively of their initial light absorption. Furthermore, the UV–visible spectra changes of these copolymers in the film state are depicted in Fig. 3. For all copolymers, a reduced absorption intensity variation of the ICT and □ – □* peaks and 94.5%, 86.5% and 74.1% of their initial light

absorption characteristics for PIDTT-DTNT-C16, PIDTT-DTNT-HD and PIDTT-DTNT-OD after 11 h of illumination in air were observed, which is in accordance with the results from XRD and DFT analyses, since the shortened and linear flexible side chain promoted dense and ordered packing, which perhaps suppressed the chance of triplet formation and impeded the diffusion of photo-oxidizing chemicals (such as oxygen and/or photoinduced radicals) into the stacked polymer chains.[72,73] Obviously, the side chain had little impact on photostability in solution but had a pronounced influence in films of the studied polymers.

XRD properties

XRD analyses for the pristine polymers PIDTT-DTNT-C16, PIDTT-DTNT-HD and PIDTT-DTNT-OD and the corresponding polymer/$PC_{61}BM$ blend films were employed to probe the impact of the side chain on crystallinity and molecular packing in the solid state. Note that these thin films were prepared through casting from CB onto glass substrates. As indicated in Fig. 4(a), only PIDTT-DTNT-C16 bearing a long branched side chain exhibited two weak peaks, but PIDTT-DTNT-HD and PIDTT-DTNT-OD showed one peak. The observed broad diffraction peaks in the wide angle region reflecting the □ – □ stacking distance were located at of 23.70°, 22.92° and 22.24° for PIDTT-DTNT-C16, PIDTT-DTNT-HD and PIDTT-DTNT-OD, respectively, corresponding to □–□ stacking distances of 3.75, 3.88 and 3.99 Å according to Bragg's law (i.e. □ = 2*d*sin□).[74] The peaks in the small angle region were located at 2□ = 4.84° for PIDTT-DTNT-C16, corresponding to a distance of the polymer backbone separated by the flexible side chain which was 18.23 Å. For the blend films, no obvious diffraction peak was observed in the PIDTT-DTBT-C16:$PC_{61}BM$ film, PIDTT-DTNT-HD:$PC_{61}BM$ showed one strong diffraction peak at 2□ = 20.14° and PIDTT-DTNT-OD:$PC_{61}BM$ exhibited one weak diffraction peak at 2□ = 22.46°, corresponding to □ – □ stacking distances of 4.40 Å for PIDTT-DTNT-HD:$PC_{61}BM$ and 3.95 Å for PIDTT-DTNT-OD:$PC_{61}BM$. Clearly, the □ – □ stacking interaction decreased gradually in the film of pure polymer; however, the blend film exhibited gradually enhanced □–□ stacking interaction when the side chain changed from C16 to HD and to OD.

Electrochemical properties

The electronic energy levels of the polymers are a crucial parameter of their PV application. The cyclic voltammetry (CV) method has been widely employed to measure the oxidation onset potentials ($□_{ox}^{onset}$) of polymers and to estimate their E_{HOMO} and E_{LUMO}. To evaluate the impact of the side chain on energy levels, the corresponding CV curves for each copolymer film on a glass carbon electrode were recorded (Fig. 5(a)), and the detailed electrochemical data are listed in Table 2. The $□_{ox}^{onset}$ values for PIDTT-DTNT-C16, PIDTT-DTNT-HD and PIDTT-DTNT-DTNT-OD were observed at 0.68, 0.68 and 0.70 V, respectively. Note that the CV curve is measured with regard to the potential of a standard $Ag/AgNO_3$ electrode calibrated with a ferrocene/ferrocenium (Fc/Fc^+) redox couple. The $□_{1/2}$ of the Fc/Fc^+ redox couple is determined to be 0.12 V *versus* the $Ag/AgNO_3$ reference electrode under identical conditions. Considering that the redox potential of Fc/Fc^+ is −4.8 eV relative to the vacuum energy level, E_{HOMO} can be calculated using $E_{HOMO} = -e(□_{ox}^{onset} + 4.68)$ (eV).[64,76] Consequently, the corresponding E_{HOMO} valus were approximately −5.36, −5.36 and −5.38 eV for PIDTT-DTNT-C16, PIDTT-DTNT-HD and PIDTT-DTNT-OD, respectively. These relatively low-lying E_{HOMO} values which were close to −5.40 eV for the ideal polymer were expected to acquire a higher V_{OC} theoretically.[29] Since □ electrons are prone to delocalize in a planar structure and to localize in a twisted structure, PIDTT-DTNT-OD exhibited a deepened E_{HOMO}; this trend was consistent with the decreased planarity from DFT calculation (later).[29] Additionaly, based on E_g^{opt} and E_{HOMO}, the E_{LUMO} values were thus estimated to be −3.69, −3.71 and −3.72 eV for PIDTT-DTNT-C16, PIDTT-DTNT-HD and PIDTT-DTNT-OD, respectively, using the equation $E_{LUMO} = E_{HOMO} + E_g^{opt}$. For better comparison, the energy level diagram of the resultant donor copolymers and $PC_{61}BM$ is shown in Fig. 5(b). It is clear that the side chain produced an insignificant impact on the energy levels. All polymers exhibited a suitable E_{LUMO} matched well with $PC_{61}BM$ and had LUMO gaps of about 0.48–0.51 eV, supporting enough driving force to realize exciton splitting and charge dissociation at the D–A interfaces, hence ensuring energetically beneficial electron transfer in order to conquer the binding energy for the intrachain exciton.[75]

Theoretical calculations

To better understand the electron distribution and the backbone conformation of the side chain type in the studied polymers, calculations were performed by DFT calculation on the B3LYP/6-31G* basis set, as executed in the Gaussian 09 program suite which was a quantum chemical program.[77] Considering the negligible impact on electron properties, the hexyl of IDTT was substituted with methyl, and the linear *n*-hexadecyl and branched 2-hexyldecyl/2-cotyl-dodecyl were replaced by *n*-butyl and iso-butyl, respectively, for simplicity. One repeating unit (unimer), denoted IDTT-DTNT-C16 and IDTT-DTNT-HD/OD, was selected as the corresponding model compound. As illustrated in Fig. 6, the HOMO orbitals are delocalized over the entire oligomer; in contrast, the LUMO orbitals are preferentially localized on the electron-deficient NT and bilateral thiophene bridges. It should be noted that the bridging sp^3-carbon prevented the electron orbital interaction between the alkylphenyl side chain and the polymeric conjugated backbone, which did not contribute to the electron delocalization of the polymer; this was consistent with the observations from other groups.[45,46] Furthermore, the calculated E_{HOMO}, E_{LUMO} and E_g are −4.71, −2.86 and 1.85 eV for PIDTT-DTNT-C16 and −4.75, −2.87 and 1.88 eV for PIDTT-DTNT-HD/PIDTT-DTNT-OD. As a whole, the trend in energy level is in accordance with the results from CV measurements. It has been demonstrated that the good planarity for the polymer backbone is instrumental in intrinsic □–□ stacking, hence facilitating excellent charge carrier mobility.[24] Consequently, the dihedral angle $□_1$ between IDTT and the alkylthiophene bridge and the dihedral angles $□_2$ and $□_3$ between the alkylthiophene bridge and the NT moiety are shown in Fig. S13 in Appendix S1. These dihedral angles $□_1$, $□_2$ and $□_3$ were 18.56°, −5.04° and −1.88° for PIDTT-DTNT-C16 and −28.93°, 6.47° and 0.11° for PIDTT-DTNT-HD/PIDTT-DTNT-OD, respectively, indicating that the planarity decreased when the side chain changed from linear C16 to branched HD/OD. It should be noted that all calculated data are higher in energy than those from experimental measurements, because only finite unimer and short side chains are taken into consideration in the DFT model to replace the CPs in our calculation process. Nevertheless, these calculation results by and large tally with the trends seen from experiment and still disclose the mutuality between molecular structure, optoelectronic properties and thus PV properties.

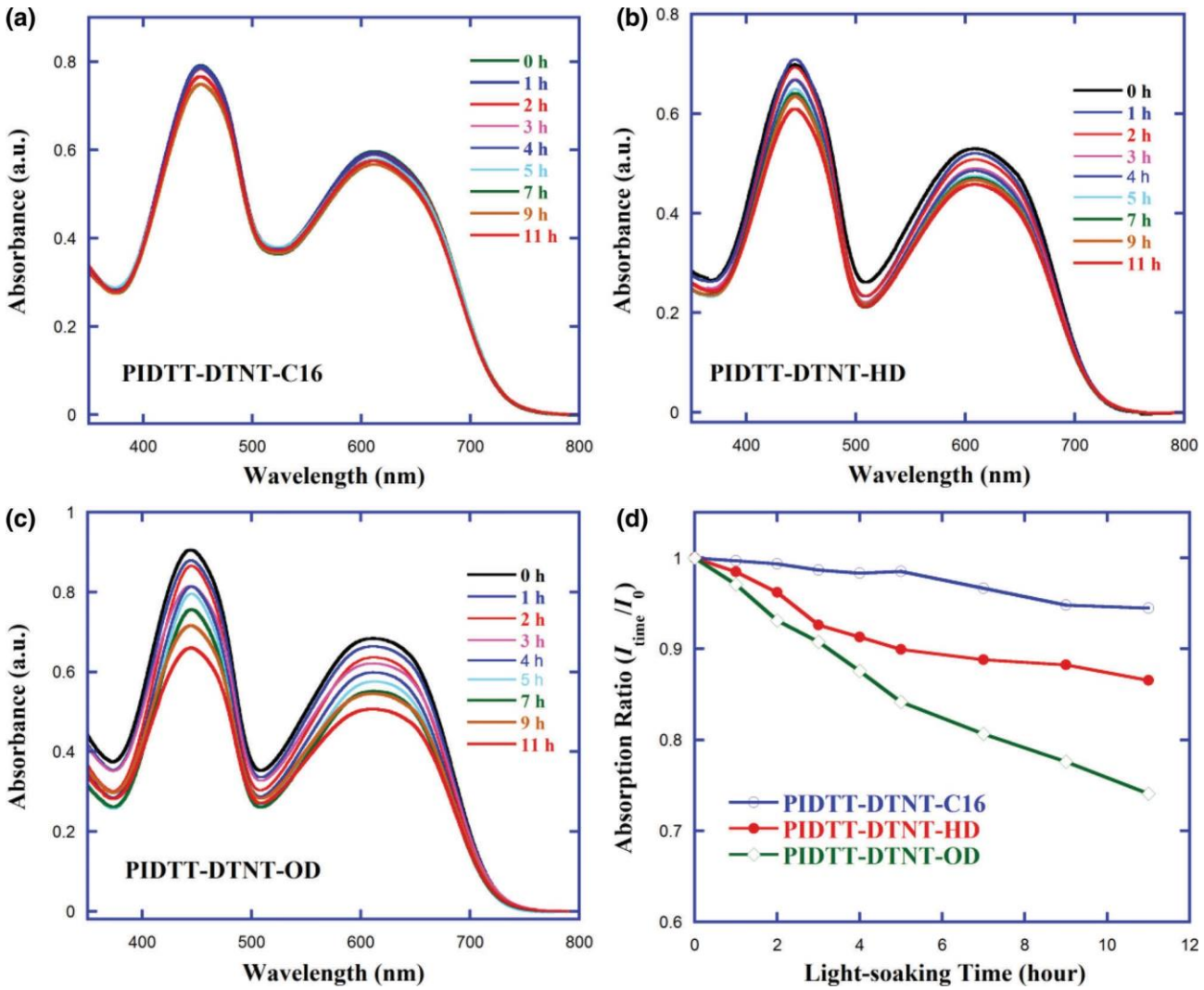

Figure 3. UV–visible absorption spectra changes after illumination of PIDTT-DTNT-C16 (a), PIDTT-DTNT-HD (b) and PIDTT-DTNT-OD (c) films on ITO, and a summary of light absorption intensity changes at the peak (*ca* 620 nm) of each polymer as a function of light-soaking time (d).

Table 2. The optimized PV parameters of PSCs under AM 1.5G illumination

Polymer	V_{OC} (V)	J_{SC} (mA cm^{-2})	FF (%)	PCE (%)	R_{SH}[b] (Ω cm^2)	R_S[b] (Ω cm^2)
PIDTT-DTNT-C16/$PC_{61}BM$	0.83	4.67 (4.56)[a]	33.56	1.30	310	77
PIDTT-DTNT-HD/$PC_{61}BM$	0.83	9.35 (9.27)[a]	42.80	3.31	257	26
PIDTT-DTNT-OD/$PC_{61}BM$	0.80	3.70 (3.61)[a]	34.41	1.02	388	100

[a] The values in parentheses are the integrated currents obtained from the EQE curves.
[b] Shunt resistance (R_{SH}) and series resistance (R_S) are deduced from the inverse slope at $V = 0$ and $V = V_{OC}$ in the J–V curves under illumination.

Photovoltaic properties

To examine the influence of the side chain on PV performance, inverted BHJ PSCs with a structure of ITO/PFN/polymers:$PC_{61}BM$/MoO_3/Ag were fabricated.[78] A 10 nm thick alcohol-soluble PFN was chosen as a cathode interfacial modifier between the ITO and active layer, which can effectively further the interfacial contact and electron extraction between the active layer and metallic cathode.[79] An 8 nm thick MoO_3 was chosen as the anode interlayer modifier between the active layer and Ag electrode. The corresponding active layers were prepared by spin-coating from the CB solution involved in PIDTT-DTNT-C16, PIDTT-DTNT-HD and PIDTT-DTNT-OD and $PC_{61}BM$. The J–V measurements were performed in simulated solar light at 100 mW cm^{-2} under AM 1.5G illumination. The initial device optimization was carried out by screening the weight ratios of these studied polymers:$PC_{61}BM$ of 1:1, 1:1.5 and 1:2. The best PV performance was observed from the devices on the basis of a polymer to $PC_{61}BM$ weight ratio of 1:1.5, and the corresponding J–V curves are exhibited in Fig. S14 in Appendix S1; detailed PV data are listed in Table S3. It is seen that the device based on PIDTT-DTNT-C16 showed the best PCE of 1.01%, with a V_{OC} of 0.84 V, a J_{SC} of 3.79 mA cm^{-2} and an FF of 31.54%, and the PIDTT-DTNT-HD-based device exhibited

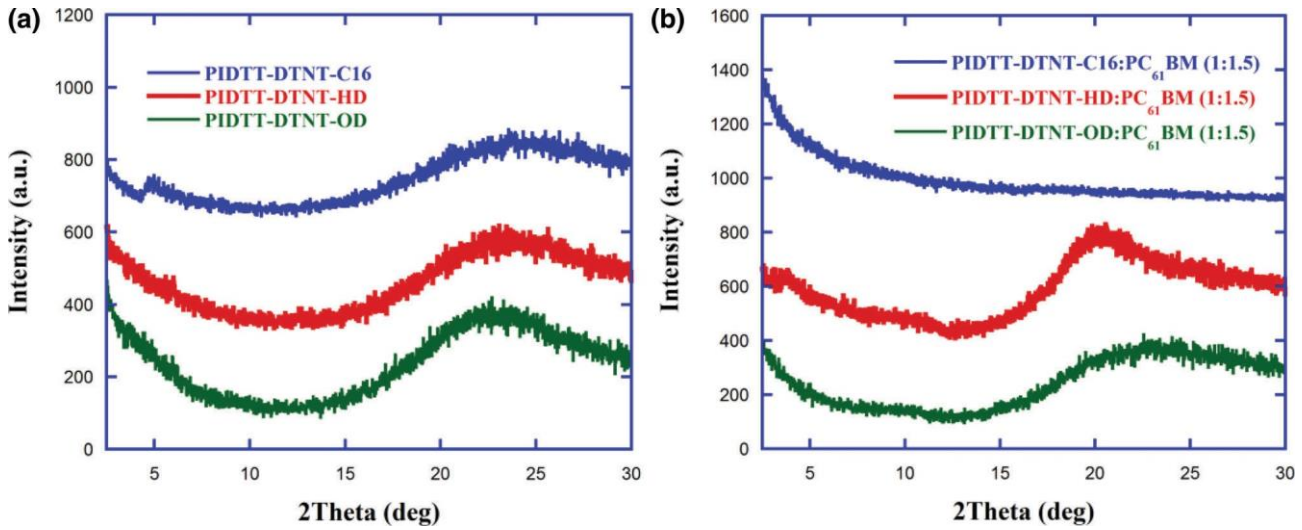

Figure 4. XRD patterns of the studied pure copolymers (a) and the blends (b) (polymer:$PC_{61}BM$ = 1:1.5).

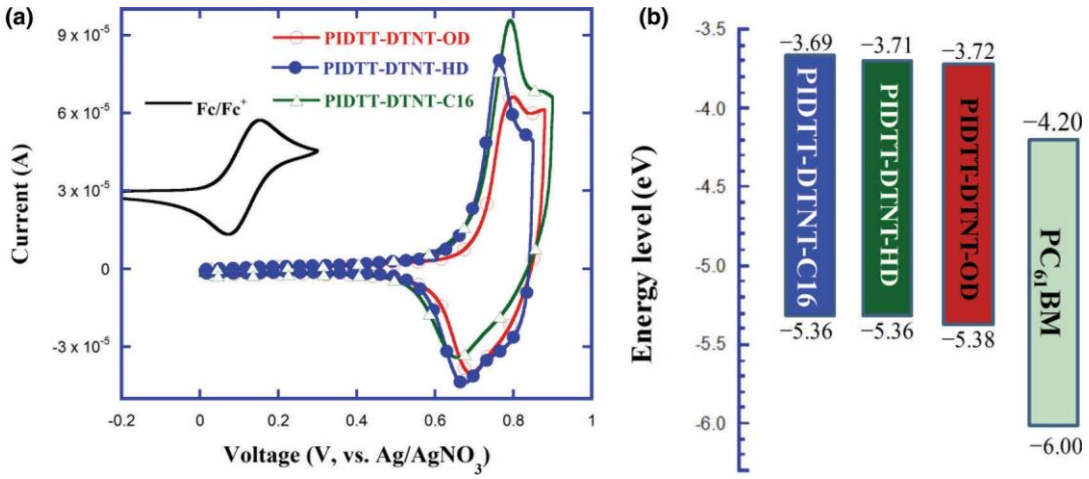

Figure 5. CV curves (a) and energy level schematic diagram (b) of copolymers PIDTT-DTNT-C16, PIDTT-DTNT-HD and PIDTT-DTNT-OD.

a relatively higher PCE of 1.86%, with a V_{OC} of 0.81 V, a J_{SC} of 5.53 mA cm^{-2} and an FF of 41.59%, but the PIDTT-DTNT-OD-based device exhibited the lowest PCE of 0.36%, with a V_{OC} of 0.78 V, a J_{SC} of 1.51 mA cm^{-2} and an FF of 30.97%. It is clear that, with the side chain branching and lengthening, the PCE exhibited a decreased variation. The relatively low-lying E_{HOMO} made these devices containing PIDTT-DTNT-based polymers acquire a higher V_{OC} ranging from 0.78 to 0.84 V. These terrible PCEs were mainly restricted by the lower J_{SC} and FF. The J_{SC} variations were confirmed by the corresponding external quantum efficiency (EQE) spectra (Fig. S14); in particular, the EQE values in the range 500–750 nm were smaller than those ranging from 300 to 500 nm, which coincided with the former absorption spectra of the copolymers.

Many investigations have verified that the solvent additive 1,8-diiodoctane (DIO) having a higher boiling point than the processing solvent CB can improve the morphology of the active layers for BHJ PSCs to raise the PV performance.[24,80] Accordingly, we utilized 3% DIO (DIO/CB, v/v) as the solvent additive during the device-fabricating process in order to further maximize the PCE of the devices. The *J*–*V* curves are outlined in Fig. S14 in Appendix S1 and detailed data are also listed in Table S3. It was observed that the PIDTT-DTNT-C16-based device exhibited a small enhanced PCE from 1.01% to 1.30% after utilizing DIO, mainly benefitting from slightly increased J_{SC} (from 3.79 to 4.67 mA cm^{-2}) and FF (31.54% to 33.56%). For PIDTT-DTNT-HD-based devices, it was found that the PCE was greatly enhanced from 1.86% to 3.31%, corresponding to largely elevated J_{SC} (from 5.53 to 9.35 mA cm^{-2}) and slightly increased FF (41.59% to 42.80%) as well as slightly maximized V_{OC} (from 0.81 to 0.83 V). As for the PIDTT-DTBT-OD-based device, the PCE was again found to be increased from 0.36% to 1.02%, which primarily originated from synchronously raised V_{OC} (from 0.78 to 0.80 V), J_{SC} (from 1.51 to 3.70 mA cm^{-2}) and FF (30.97% to 34.41%). These dramatically increased J_{SC} were confirmed by EQE evaluations, as shown in Fig. S14. Obviously, PIDTT-DTNT-C16 containing a linear side chain exhibited the smallest enhancement and the copolymers involving branched chains produced the larger improvements. As is known, larger shunt resistances (R_{SH}) and smaller series resistances (R_S) were beneficial to gaining higher FF. Thus R_{SH} and R_S values calculated from the *J*–*V* curves of devices at $V = 0$ and $V = V_{OC}$, respectively, are listed in Table S3. In detail, these decreased R_S values (from 100 to 77 Ω cm^2 for PIDTT-DTNT-C16, from 43 to 26 Ω cm^2 for PIDTT-DTNT-HD and from 583 to 100 Ω cm^2 for PIDTT-DTNT-OD) can well account for the corresponding relatively small enhancements in FF (31.54% to

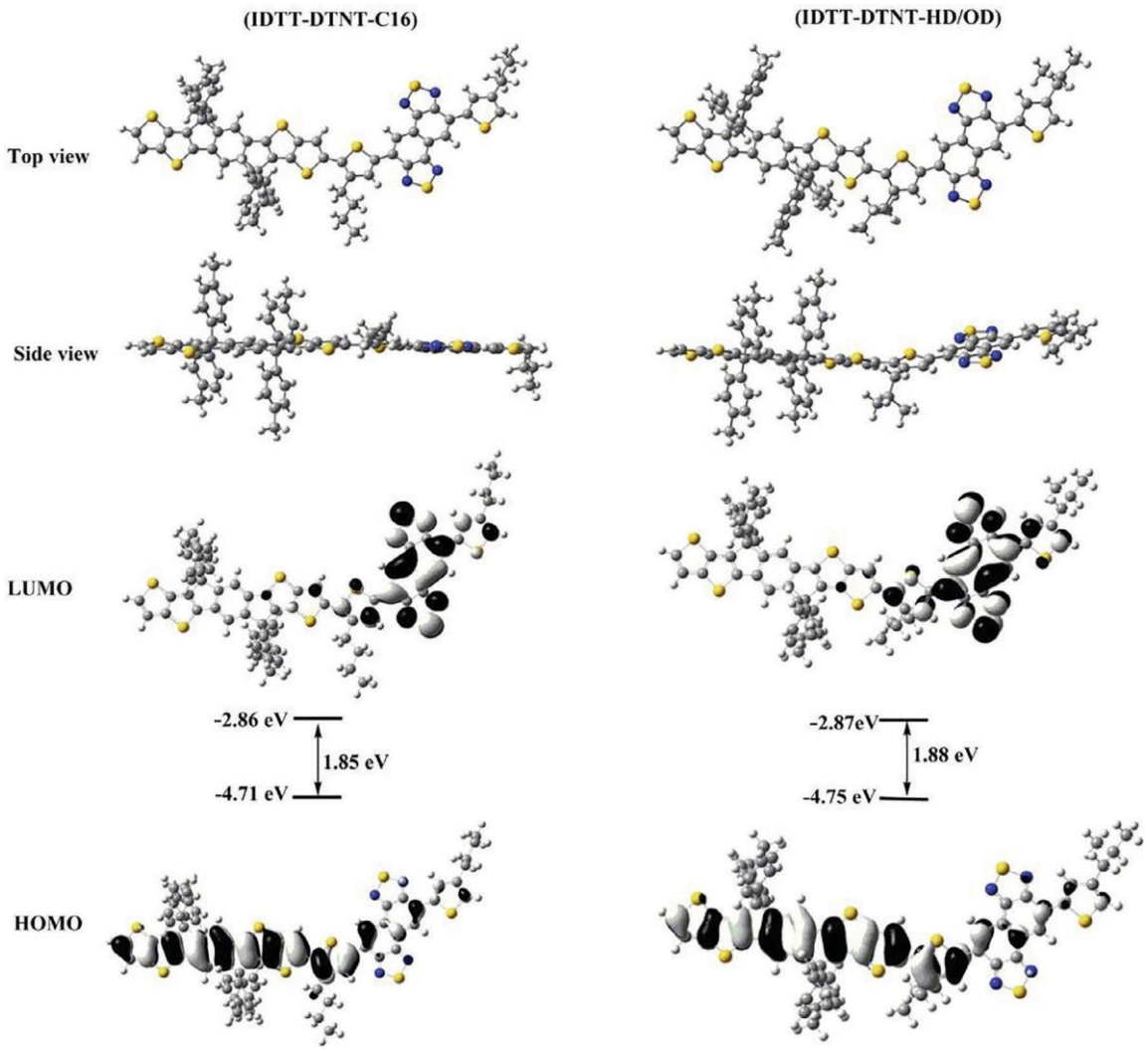

Figure 6. Optimized geometries and molecular orbital surfaces of the HOMO and LUMO for the unimer model compound, obtained with the B3LYP/6-31G* basis set.

33.56% for PIDTT-DTNT-C16, 41.59% to 42.80% for PIDTT-DTNT-HD and 30.97% to 34.41% for PIDTT-DTNT-OD).

Assisted by D/A ratio screening and DIO additive utilization, the best *J–V* curves and EQE spectra of the studied copolymers are shown in Fig. 7 and the optimized PV data are listed in Table 2. We can see that the optimal PCE increased from 1.30% to 3.31% when the side chain changed from linear C16 to branched HD, chiefly benefitting from a 100% increase in J_{SC} (from 4.67 to 9.35 mA cm^{-2}) and 27.53% enhancement in FF (from 33.56% to 42.80%) even with an unchanged V_{OC}. Subsequently, after the side chain was further prolonged to OD, the PCE largely declined to about 69.2% (from 3.31% to 1.02%), which was primarily ascribed to simultaneous 3.6% (from 0.83 to 0.80 V), 60.4% (from 9.35 to 3.70 mA cm^{-2}) and 19.6% (from 42.80% to 34.41%) deteriorations for the corresponding V_{OC}, J_{SC} and FF of the devices. The variations of J_{SC} were validated by the corresponding EQE curve (Fig. 7(b)). The PIDTT-DTNT-C16-based device exhibited low EQE response (smaller than 20%) in the range 520 – 750 nm; meanwhile the PIDTT-DTNT-HD-based device showed an obviously improved EQE (between 40% and 60%) over the whole response range (300 – 750 nm). As for the PIDTT-DTNT-OD-based device, the EQE profile was similar to that of PIDTT-DTNT-HD but the response was inferior. Also, integrated J_{SC} values from the EQE curves were 4.56, 9.27 and 3.61 mA cm^{-2} for the best-performing PIDTT-DTNT-C16:$PC_{61}BM$, PIDTT-DTNT-HD:$PC_{61}BM$ and PIDTT-DTNT-OD:$PC_{61}BM$, respectively, indicative of an error of less than 5% compared to the J_{SC} values from *J–V* tests. Moreover, the variations in FF were confirmed by the trend of first decreasing and then increasing R_S (from 77 to 26 then to 100 Ω cm^2) after the flexible side chain was changed from C16 to HD and then to OD. All in all, the PIDTT-DTNT-HD exhibited at least a 1.53-fold enhancement in PCE compared to the polymers bearing C16 and OD side chains.

Hole mobility

It has been demonstrated that charge mobility undoubtedly plays an important role in affecting the PV performance because it is directly related to charge transport and recombination.[14,81,82] In order to further assess the vertical hole transport character of these copolymers, hole-only and electron-only devices of polymer:$PC_{61}BM$ blend films were fabricated with the device configurations of ITO/poly(3,4-ethylenedioxythiophene):poly(styrenesulfonate) (PEDOT:PSS)/

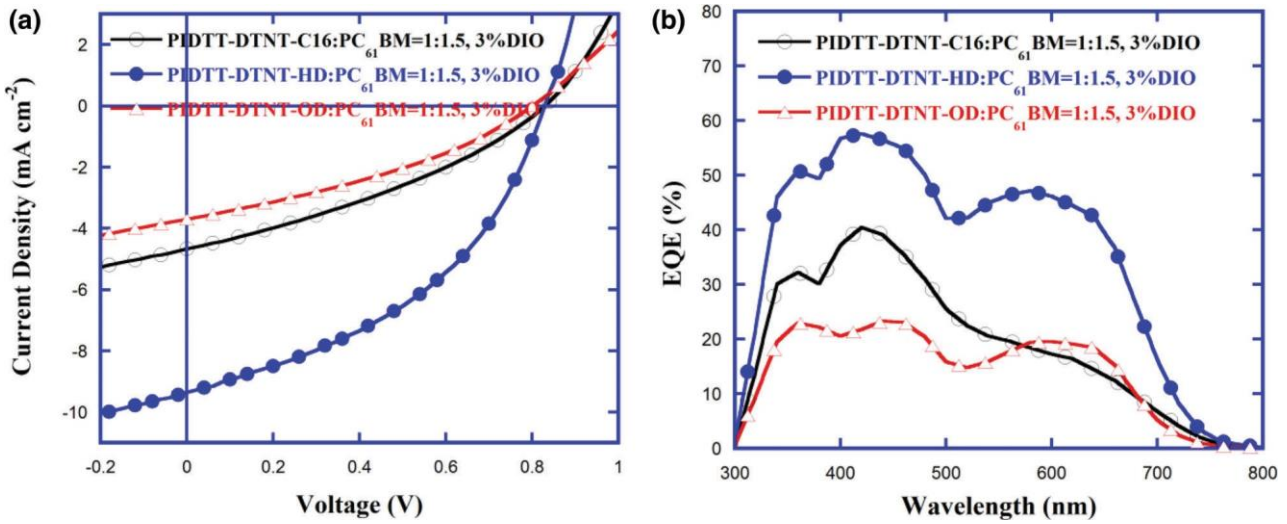

Figure 7. The optimized *J* – *V* curves (a) and the EQE spectra (b) for the PSCs based on the studied copolymers containing different side chains.

blend/MoO_3/Ag and ITO/ZnO/blend/MoO_3/Al under identical conditions of the corresponding optimized PSCs. Note that the thicknesses of PIDTT-DTNT-C16, PIDTT-DTNT-HD and PIDTT-DTNT-OD were 114, 133 and 137 nm for hole-only devices and 95, 125 and 120 nm for electron-only devices, respectively. The *J*–*V* and $J^{1/2}$–*V* characteristics for the blend films were obtained in the dark for hole-only and electron-only devices, as shown in Fig. S15 and Fig. 8, respectively. It is shown that the hole mobility (μ_h) and electron mobility (μ_e) are 1.47×10^{-4} and 4.60×10^{-7} for PIDTT-DTNT-C16, 1.10×10^{-5} and 6.48×10^{-7} for PIDTT-DTNT-HD and 1.37×10^{-5} and 6.60×10^{-5} $cm^2 V^{-1} s^{-1}$ for PIDTT-DTNT-OD (Tables S4 and S5), respectively. Clearly, the hole mobility showed a decreasing tendency; however, the electron mobility exhibited first an enhanced and then a decreased trend when the side chain was changed from linear C16 to the branched HD and OD. Furthermore, from Table 3, the values of the μ_h/μ_e ratio are 319.5 for PIDTT-DTNT-C16, 16.9 for PIDTT-DTNT-HD and 207.7 for PIDTT-DTNT-OD. The more balanced μ_h/μ_e observed in the PIDTT-DTNT-OD-based device can partially account for the higher FF and thus improved J_{SC}.[14,81–83]

Table 3. Mobility data of the studied polymers containing different side chains

Active layer	μ_h[a] ($cm^2 V^{-1} s^{-1}$)	μ_e[b] ($cm^2 V^{-1} s^{-1}$)	μ_h/μ_e
PIDTT-DTNT-C16: $PC_{61}BM$ = 1:1.5	1.47×10^{-4}	4.60×10^{-7}	319.5
PIDTT-DTNT-HD:PC_{61} BM = 1:1.5	1.10×10^{-5}	6.48×10^{-7}	16.9
PIDTT-DTNT-OD:PC_{61} BM = 1:1.5	1.37×10^{-5}	6.60×10^{-8}	207.7

[a] Hole-only devices with the structure of ITO/PEDOT:PSS/polymer: $PC_{61}BM/MoO_3$/Ag.
[b] Electron-only devices with the structure of ITO/ZnO/polymer: $PC_{61}BM$/PFN/Al.

Morphological properties

The morphology of the active layer for BHJ PSCs is an important factor to determine the charge generation and the extraction properties of PSCs.[74,80,84] In order to explain why PIDTT-DTNT-HD

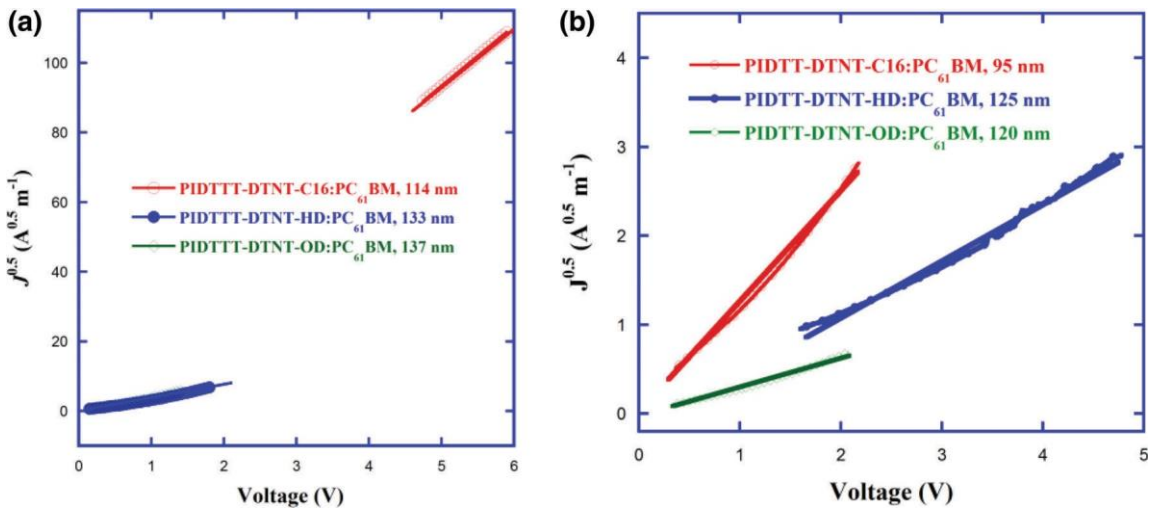

Figure 8. $J^{1/2}$ – *V* characteristics of hole-only (a) and electron-only (b) devices of the studied copolymers containing different side chains.

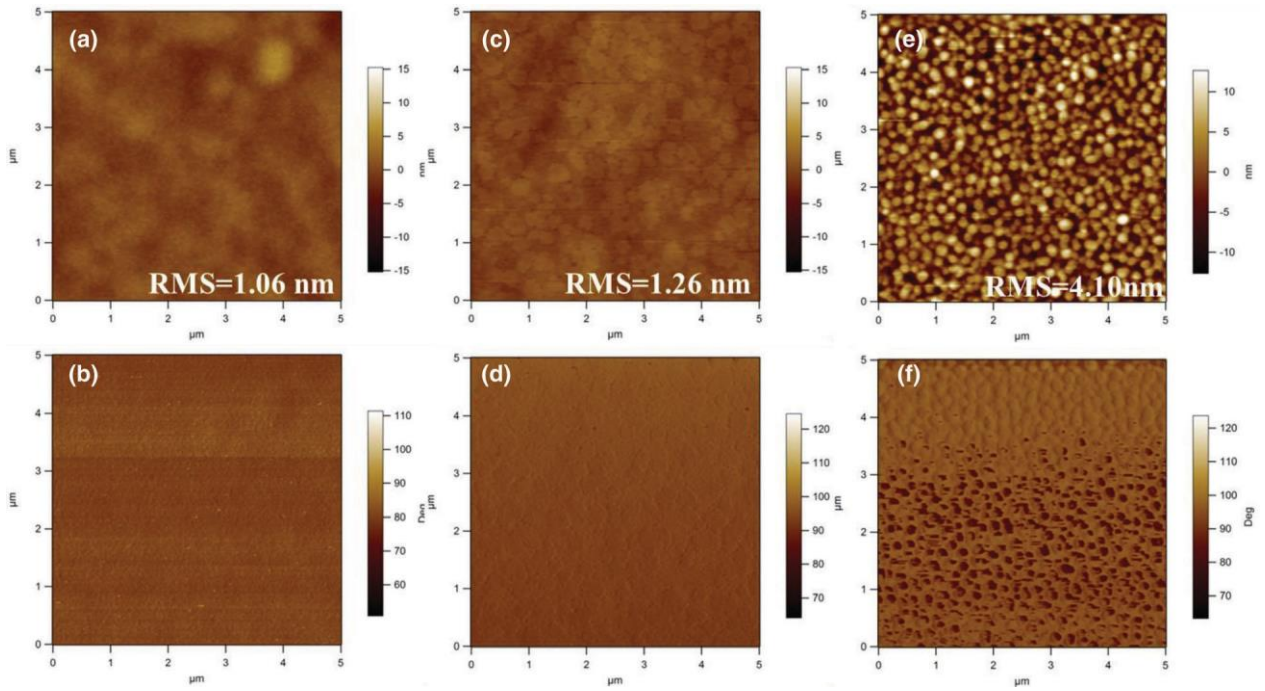

Figure 9. Tapping AFM height (upper) and phase (bottom) images of the active layers of (a), (b) PIDTT-DTNT-C16:$PC_{61}BM$ (1:1.5, 3% DIO), (c), (d) PIDTT-DTNT-HD:$PC_{61}BM$ (1:1.5, 3% DIO) and (e), (f) PIDTT-DTNT-OD: $PC_{61}BM$ (1:1.5, 3% DIO). Image size 5 × 5 μm. RMS, root mean square roughness.

Figure 10. TEM bright field images of the active layers for (a) PIDTT-DTNT-C16/$PC_{61}BM$ (1:1.5, 3% DIO), (b) PIDTT-DTNT-HD/$PC_{61}BM$ (1:1.5, 3% DIO) and (c) PIDTT-DTNT-OD/$PC_{61}BM$ (1:1.5, 3% DIO).

containing the branched HD side chain yielded a relatively enlarged PCE, we applied the tapping-model AFM measurement to examine the surface morphologies, as shown in Fig. 9. Note that all blend films were prepared under exactly the same conditions as those of the optimal device. It is shown that the root-mean-square roughness of the blend films was 3.06 nm for PIDTT-DTNT-C16:$PC_{61}BM$, 1.26 nm for PIDTT-DTNT-HD:$PC_{61}BM$ and 4.10 nm for PIDTT-DTNT-OD:$PC_{61}BM$. The gradually increased surface roughness was identical with the aggregation trend observed in the former blend film when the side chain was changed from C16 to HD to OD. It is noted that PIDTT-DTNT-OD exhibited a pinhole-like morphology, which is bad for improving the PCE. Besides, TEM was further utilized to examine the in-depth morphology of the active layers. From Fig. 10, PIDTT-DTNT-C16 exhibited poor phase separation, which cannot sufficiently support the D–A interfacial areas to promote exciton dissociation into free charges. When C16 was changed into HD and OD, the phase separation was slightly improved. The observed morphological information can partly explain the reason for the relatively higher FF and J_{SC} in the PIDTT-DTNT-HD-based device.[64,85–88]

CONCLUSION

To sum up, three D-□-A type CPs PIDTT-DTNT-C16, PIDTT-DTNT-HD and PIDTT-DTNT-OD bearing diverse flexible side chains were designed and synthesized to investigate the influence of the side chain on absorption, electrochemical properties, backbone conformation and PV properties. As a result of incorporating a medium IDTT donor unit and a strong NT acceptor into the polymer backbone, the copolymers exhibited a medium optical bandgap of *ca* 1.66 eV ranging from 300 to 750 nm and a low-lying E_{HOMO} of about −5.36 V. The side chain gave rise to an insignificant impact on the absorption, aggregation and photostability in CB solution, as well as energy levels, but a non-negligible influence on absorption, photostability and aggregation behavior in the film state. It is shown that PIDTT-DTNT-C16 possessing the densest and most ordered packing structure exhibited the best photostability. Meanwhile, PIDTT-DTNT-HD with branched HD side chain showed a 1.53 times enhancement in PCE of 3.31%, which chiefly benefitted from its slightly improved absorption, more balanced $□_h/□_e$ and morphology of the active layer as a result of introducing the branched HD side chain into the IDTT-DTNT backbone.

ACKNOWLEDGEMENTS

We are deeply grateful to the Fundamental Research Funds for the Central Universities (31920190156), Lanzhou Jiaotong University-Tianjin University Joint Innovation Fund Project Funding (2019056), the National Nature Science Foundation of China (51602139), the Natural Science Foundation of Gansu Province (18JR3RA108), the Excellent Team of Scientific Research in Lanzhou Jiaotong University (201705) and the Agricultural Science and Technology Innovation Project for Gansu Academy of Agricultural Sciences (No. 2016GAAS34) for financial support. We also express our thanks to the Instrument Analysis Center of LZJTU for the associated testing support.

SUPPORTING INFORMATION

Supporting information may be found in the online version of this article.

REFERENCES

1 Günes S, Neugebauer H and Sariciftci NS, *Chem Rev* **107**:1324 (2007).
2 Li Y, *Acc Chem Res* **45**:723 (2012).
3 Li Z, Lin H, Jiang K, Carpenter J, Li Y, Liu Y *et al.*, *Nano Energy* **15**:607 (2015).
4 Wang Y, Liang Z, Li X, Qin J, Ren M, Yang C *et al.*, *J Mater Chem C* **7**:11152 (2019).
5 Zhou H, Yang L and You W, *Macromolecules* **45**:607 (2012).
6 Yuan J, Zhang Y, Zhou L, Zhang G, Yip H-L, Lau T-K *et al.*, *Joule* **3**:1140 (2019).
7 Fan B, Zhang D, Li M, Zhong W, Zeng Z, Ying L *et al.*, *Sci China Chem* **62**:746 (2019).
8 Huo L, Liu T, Sun X, Cai Y, Heeger AJ and Sun Y, *Adv Mater* **27**:2938 (2015).
9 Wadsworth A, Moser M, Marks A, Little MS, Gasparini N, Brabec CJ *et al.*, *Chem Soc Rev* **48**:1596 (2019).
10 Dou L, You J, Yang J, Chen C-C, He Y, Murase S *et al.*, *Nat Photonics* **6**:180 (2012).
11 Zhang Z-G and Li Y, *Sci China Chem* **58**:192 (2015).
12 Mei J and Bao Z, *Chem Mater* **26**:604 (2014).
13 Zhang C, Sun Y, Dai B, Zhang X, Yang H, Lin B *et al.*, *Chin J Org Chem* **34**:1701 (2014).
14 Tong J, An L, Li J, Lv J, Guo P, Li L *et al.*, *J Polym Sci A* **56**:2059 (2018).
15 Wang X, Dou K, Shahid B, Liu Z, Li Y, Sun M *et al.*, *Chem Mater* **31**:6163 (2019).
16 Zhang Z-G and Wang J, *J Mater Chem* **22**:4178 (2012).
17 Chen W, Huang G, Li X, Li Y, Wang H, Jiang H *et al.*, *ACS Appl Mater Interfaces* **11**:33173 (2019).
18 Wu Y, Li Z, Ma W, Huang Y, Huo L, Guo X *et al.*, *Adv Mater* **25**:3449 (2013).
19 Ma Z, Sun W, Himmelberger S, Vandewal K, Tang Z, Bergqvist J *et al.*, *Energy Environ Sci* **7**:361 (2014).
20 Zhou N, Guo X, Ortiz RP, Harschneck T, Manley EF, Lou SJ *et al.*, *J Am Chem Soc* **137**:12565 (2015).
21 Wang X, Du Z, Dou K, Jiang H, Gao C, Han L *et al.*, *Adv Energy Mater* **9**:1802530 (2019).
22 Zhong W, Xiao J, Sun S, Jiang X-F, Lan L, Ying L *et al.*, *J Mater Chem C* **4**:4719 (2016).
23 Cai P, Chen Z, Zhang L, Chen J and Cao Y, *J Mater Chem C* **5**:2786 (2017).
24 Tong J, Li J, Zhang P, Ma X, Wang M, An L *et al.*, *Polymer* **121**:183 (2017).
25 Gao P, Tong J, Guo P, Li J, Wang N, Li C *et al.*, *J Polym Sci A* **56**:85 (2018).
26 Qi F, Zhang Y, Wan M, Liu J and Huo L, *J Mater Chem C* **6**:4208 (2018).
27 Chen P, Shi S, Wang H, Qiu F, Wang Y, Tang Y *et al.*, *ACS Appl Mater Interfaces* **10**:21481 (2018).
28 Wang X, Tang A, Chen F and Zhou E, *Macromolecules* **51**:4598 (2018).
29 Shi Q, Fan H, Liu Y, Chen J, Ma L, Hu W *et al.*, *Macromolecules* **44**:4230 (2011).
30 Kim J-H, Wood S, Park JB, Wade J, Song M, Yoon SC *et al.*, *Adv Funct Mater* **26**:1517 (2016).
31 Causin V, Marega C, Marigo A, Valentini L and Kenny JM, *Macromolecules* **38**:409 (2005).
32 Wang E, Hou L, Wang Z, Ma Z, Hellström S, Zhuang W *et al.*, *Macromolecules* **44**:2067 (2011).
33 Cabanetos C, Labban AE, Bartelt JA, Douglas JD, Mateker WR, Fréchet JMJ *et al.*, *J Am Chem Soc* **135**:4656 (2013).
34 Li W, Hendriks KH, Furlan A, Roelofs WSC, Meskers SCJ, Wienk MM *et al.*, *Adv Mater* **26**:1565 (2014).
35 Jin Y, Chen Z, Dong S, Zheng N, Ying L, Jiang X-F *et al.*, *Adv Mater* **28**:9811 (2016).
36 Kini GPLSK, Shin WS, Moon S-J, Song CE and Lee J-C, *J Mater Chem A* **4**:18585 (2016).
37 Liu Y, Zhao J, Li Z, Mu C, Ma W, Hu H *et al.*, *Nat Commun* **5**:5293 (2014).
38 Takimiya K, Shinamura S, Osaka I and Miyazaki E, *Adv Mater* **23**:4347 (2011).
39 Sun S, Zhang P, Li J, Li Y, Wang J, Zhang S *et al.*, *J Mater Chem A* **2**:15316 (2014).
40 Xia Y, Li Y, Zhu Y, Li J, Zhang P, Tong J *et al.*, *J Mater Chem C* **2**:1601 (2014).
41 Son HJ, Lu L, Chen W, Xu T, Zheng T, Carsten B *et al.*, *Adv Mater* **25**:838 (2013).
42 Liang C and Wang H, *Org Electron* **50**:443 (2017).
43 Xu Y-X, Chueh C-C, Yip H-L, Ding F-Z, Li Y-X, Li C-Z *et al.*, *Adv Mater* **24**:6356 (2012).
44 Cai Y, Zhang X, Xue X, Wei D, Huo L and Sun Y, *J Mater Chem C* **5**:7777 (2017).
45 Xu X, Cai P, Lu Y, Choon NS, Chen J, Ong BS *et al.*, *Macromol Rapid Commun* **34**:681 (2013).
46 Chang H-H, Tsai C-E, Lai Y-Y, Liang W-W, Hsu S-L, Hsu C-S *et al.*, *Macromolecules* **46**:7715 (2013).
47 Cai P, Xu X, Sun J, Chen J and Cao Y, *RSC Adv* **7**:20440 (2017).
48 Lee W and Jung JW, *J Mater Chem A* **5**:712 (2017).
49 Li Y, Yao K, Yip H-L, Ding F-Z, Xu Y-X, Li X *et al.*, *Adv Funct Mater* **24**:3631 (2014).
50 Wang M, Hu X, Liu L, Duan C, Liu P, Ying L *et al.*, *Macromolecules* **46**:3950 (2013).
51 Zhai W, Zhou E and Chin J, *Org Chem* **36**:2786 (2016).
52 Sun Y, Chien S-C, Yip H-L, Zhang Y, Chen K-S, Zeigler DF *et al.*, *J Mater Chem* **21**:13247 (2011).
53 Wang K, Zhao Y, Tang W, Zhang Z-G, Fu Q and Li Y, *Org Electron* **15**:818 (2014).
54 Xu Y-X, Chueh C-C, Yip H-L, Chang C-Y, Liang P-W, Intemann JJ *et al.*, *Polym Chem* **4**:5220 (2013).
55 Xu X, Li Z, Bäcke O, Bini K, James DI, Olsson E *et al.*, *J Mater Chem A* **2**:18988 (2014).
56 Intemann JJ, Yao K, Li Y-X, Yip H-L, Xu Y-X, Liang P-W *et al.*, *Adv Funct Mater* **24**:1465 (2014).
57 Wang Y and Michinobu T, *J Mater Chem C* **4**:6200 (2016).
58 Wang M, Hu X, Liu P, Li W, Gong X, Huang F *et al.*, *J Am Chem Soc* **133**:9638 (2011).
59 Osaka I, Shimawaki M, Mori H, Doi I, Miyazaki E, Koganezawa T *et al.*, *J Am Chem Soc* **134**:3498 (2012).
60 Zhang M, Zhu L, Guo P, Wang X, Tong J, Zhang X *et al.*, *Polymers* **11**:239 (2019).
61 Tong J, An L, Li J, Zhang P, Guo P, Yang C *et al.*, *J Macromol Sci A* **54**:176 (2017).
62 Guo P, Xia Y, Huang F, Luo G, Li J, Zhang P *et al.*, *RSC Adv* **5**:12879 (2015).
63 Kawashima K, Fukuhara T, Suda Y, Suzuki Y, Koganezawa T, Yoshida H *et al.*, *J Am Chem Soc* **138**:10265 (2016).
64 Tong J, An L, Lv J, Guo P, Wang X, Yang C *et al.*, *Polymers* **11**:12 (2019).
65 Huang F, Wu H, Wang D, Yang W and Cao Y, *Chem Mater* **16**:708 (2004).
66 Xia Y, Gao Y, Zhang Y, Tong J, Li J, Li H *et al.*, *Polymer* **54**:607 (2013).
67 Guo X, Zhou N, Lou SJ, Smith J, Tice DB, Hennek JW *et al.*, *Nat Photonics* **7**:825 (2015).
68 Carsten B, He F, Son HJ, Xu T and Yu L, *Chem Rev* **111**:1493 (2011).
69 Blouin N, Michaud A and Leclerc M, *Adv Mater* **19**:2295 (2007).
70 Jørgensen M, Norrman K, Gevorgyan SA, Tromholt T, Andreasen B and Krebs FC, *Adv Mater* **24**:580 (2012).
71 Rivaton A, Tournebize A, Gaume J, Bussière P-O, Gardette J-L and Therias S, *Polym Int* **63**:1335 (2014).
72 Lee HS, Song HG, Jung H, Kim MH, Cho C, Lee J-Y *et al.*, *Macromolecules* **49**:7844 (2016).
73 Soon YW, Cho H, Low J, Bronstein H, McCulloch I and Durrant JR, *Chem Commun* **49**:1291 (2013).
74 Li G, Zhao B, Kang C, Lu Z, Li C, Dong H *et al.*, *ACS Appl Mater Interfaces* **7**:10710 (2015).
75 Xu T and Yu L, *Mater Today* **17**:11 (2014).
76 Pommerehne J, Vestweber H, Guss W, Mark RF, Bässles H, Porsch M *et al.*, *Adv Mater* **7**:551 (1995).

77 Frisch MJ, Trucks GW, Schlegel HB, Scuseria GE, Robb MA, Cheeseman JR *et al.*, *Gaussian 09, Revision A.01*. Gaussian Inc., Wallingford, CT (2009).
78 He Z, Zhong C, Su S, Xu M, Wu H and Cao Y, *Nat Photonics* **6**:591 (2012).
79 He Z, Zhang C, Xu X, Zhang L, Huang L, Chen J *et al.*, *Adv Mater* **23**:3086 (2011).
80 Wang N, Chen W, Shen W, Duan L, Qiu M, Wang J *et al.*, *J Mater Chem A* **4**:10212 (2016).
81 Liang Z, Tong J, Li H, Wang Y, Wang N, Li J *et al.*, *J Mater Chem A* **7**:15841 (2019).
82 Li J, Wang Y, Liang Z, Wang N, Tong J, Yang C *et al.*, *ACS Appl Mater Interfaces* **11**:7022 (2019).
83 Bao X, Zhang Y, Wang J, Zhu D, Yang C, Li Y *et al.*, *Chem Mater* **29**:6766 (2017).
84 Aghapour S, Agbolaghi S, Charoughchi S, Sarvari R and Abbasi F, *Polym Int* **68**:64 (2019).
85 Chen W, Shen W, Wang H, Liu F, Duan L, Xu X *et al.*, *Dyes Pigm* **166**:42 (2019).
86 Zhu D, Zhu Q, Gu C, Ouyang D, Qiu M, Bao X *et al.*, *Macromolecules* **49**:5788 (2016).
87 Li J, Liang Z, Wang Y, Li H, Tong J, Bao X *et al.*, *J Mater Chem C* **6**:11015 (2018).
88 Wang Y, Liang Z, Qin J, Tong J, Guo P, Cao X *et al.*, *IEEE J Photovoltaics* **9**:1678. (2019). https://doi.org/10.1109/JPHOTOV.2019.2941828.